# Pareto Optimization of Circular Power Pads for Contactless Electric Vehicle Battery Charger

Masood Moghaddami, Arash Anzalchi, Amir Moghadasi and Arif Sarwat
Electrical and Computer Engineering, Florida International University, Miami, Florida 33174, Email: asarwat@fiu.edu

***Abstract*—Design optimization of circular power pads for inductive power transfer (IPT) systems with applications in electric vehicle battery charger is proposed. A multi-objective optimization coupled with 2D finite element analysis (FEA) is used to find the Pareto-optimal solutions for circular magnetic structures considering different objective functions, such as power transfer efficiency, material cost, and horizontal misalignment tolerance of the IPT system. 2D FEA is used to calculate self and mutual inductances between primary and secondary pads, ohmic loss in coils, core loss in ferrites, stray loss in aluminum shields and electromagnetic field (EMF) emissions of the system. Practical limitations of the power electronic converters such as frequency, VA rating, operating quality factor, and EMF emissions are all considered in the proposed optimization. A 10 kW electric vehicle battery charger IPT system with circular power pads is investigated as the case study and Pareto-optimal solutions for this system are presented. Experimental test results on one of the Pareto-optimal solutions are in good agreement with the calculations using the proposed method. The proposed design optimization method provides a tool for finding highly efficient, flexible and cost-effective solutions for contactless electric vehicle battery charger.**

***Index Terms*—electric vehicle, finite element analysis, inductive power transfer, optimization.**

## NOMENCLATURE

| | |
|---|---|
| $A$ | Magnetic vector potential $(V.s/m)$ |
| $H$ | Magnetic field $(A/m)$ |
| $B$ | Magnetic flux density $(Tesla)$ |
| $J$ | Eddy-current density $(A/m^2)$ |
| $\omega$ | Frequency $(rad/s)$ |
| $\mu$ | Magnetic permeability $(H/m)$ |
| $\nu$ | Magnetic reluctivity $(m/H)$ |
| $\sigma$ | Electrical conductivity $(S/m)$ |
| $P$ | Power loss $(W)$ |

## I. INTRODUCTION

INDUCTIVE power transfer (IPT) technology is a widely accepted technique for transferring power without any physical contacts. This technology transfers power from one system to another across a relatively large air gap between two loosely coupled inductors, which have a weak magnetic coupling. Since it is unaffected by dust or chemicals and eliminates sparking and the risk of electrical shock, it can be used in hazardous environments. This technology offers high reliability, robustness and high efficiency, typically between 85–90%. Therefore, it provides a clean, safe and robust way of transferring power and has rapidly gained increased interest in the industrial and commercial sectors. The IPT technology has been successfully employed in many applications, including systems for materials handling [1], [2], biomedical implants [3], [4] and transportation systems [5]. Specifically this innovative technology can be used for static and dynamic electric vehicle (EV) charging [6], [7].

This work was funded by the National Science Foundation under grant number CRISP-1541108.

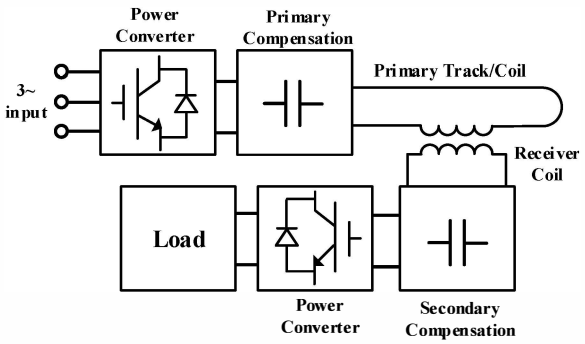


Fig. 1. A typical loosely coupled IPT system.

In a loosely coupled IPT system, due to weak coupling of the coils in an inductive link, it requires a strong magnetic field to be created to deliver high power levels at large ranges. To achieve this, it requires the use of a reactive power compensation circuit, as well as power converters that can generate large currents at high frequencies, often in the kilohertz ranges. In order to generate a high-frequency current on the primary side, power converters are employed in IPT systems. A typical configuration of an IPT system is shown in Fig. 1. The power source of an IPT system is usually the electric utility ($1\phi$ or $3\phi$) supplying power at 50/60 Hz, though for portable applications a dc battery source may be used [2].

Efficiency of an IPT system is one of the key parameters that should be considered as a design measure. Although in low-power IPT applications, efficiency might not be critical, in high-power IPT systems, such as electric vehicle fast charging, due to thermal limitations of the components the efficiency of the system is critical. Another important aspect of an IPT system is its cost efficiency. The efficiency of an IPT system with circular power pads can be increased by adding low-loss ferrites with high permeability to the structure of the circular pads. However, the addition of ferrites will increase the cost of the power pads significantly. Therefore, special attention needs to be paid to the cost efficiency of the magnetic structure.

An unguided vehicle parking requires a large charging zone for more convenience. Therefore, high tolerance to horizontal displacement in an IPT system is essential for a convenient vehicle charging. This tolerance is specified to be between $\pm$100 mm and $\pm$150 mm or higher [8]. Thus, the power pads should be designed in a way that have an acceptable horizontal displacement tolerance. However, a magnetic structure with high horizontal displacement tolerance may not be a cost-efficient solution. Due to complexity of the magnetic structures in IPT systems, finding analytical solutions for the electromagnetic field computation is very complex and cumbersome [9]. Therefore, finite element analysis (FEA) is usually used in order to compute the magnetic field distribution, and thereby, different parameters such as, self and mutual inductances of the power pads, power losses in the coils, ferrite cores and shielding plate, as well as electromagnetic field emissions (EMF) [10]–[14].

In this paper, multi-objective optimization of circular power pads for IPT systems is studied. The optimization is performed on the structure of circular power pads to maximize the efficiency and horizontal misalignment capability and minimize the total cost of the power pad simultaneously. For this purpose, a multi-objective genetic algorithm (GA), which is coupled with 2D finite element analysis (FEA), is used. 2D FEA is used for calculation of magnetic coupling, as well as electromagnetic field emissions (EMF) of the IPT system. A 10 kW case study IPT system design using the proposed multi-objective optimization is implemented and the results are compared to the theoretical calculation results.

The optimal power pad structures can be selected between different Pareto-optimal solutions for IPT systems by prioritizing the different objective functions. Co-optimization of primary and secondary magnetic structures is performed using the multi-objective genetic algorithm (GA) coupled with the 2D FEA. EMF emissions of the pads are defined as constraints for the optimization method to meet human exposure regulations in compliance with standards, as defined by International Commission on Non-Ionizing Radiation Protection (ICNIRP). Furthermore, the operational quality factor (Q) of the primary and secondary pads should be within the limits of primary and secondary power converters.

## II. Circular Power Pads

Various topologies for magnetic structures in IPT systems are proposed. These structures include U-cores [15], [16], E-cores [16], [17], S-cores [17], pot-cores [18], [19], and ferrite discs or plates [20]. Because of the use of large ferrite cores in these structures, they are relatively bulky, expensive, and fragile. On the other hand, the space for the receiver coil under the EV and the admissible weight of the magnetic structures are normally limited, and therefore the weight and volume of the IPT magnetic structures should be considered. Therefore, conventional structures may compromise the ground clearance of the EV or require major chassis adjustment.

In this study, circular power pads, which are the most common magnetic structures used in IPT systems, are considered.

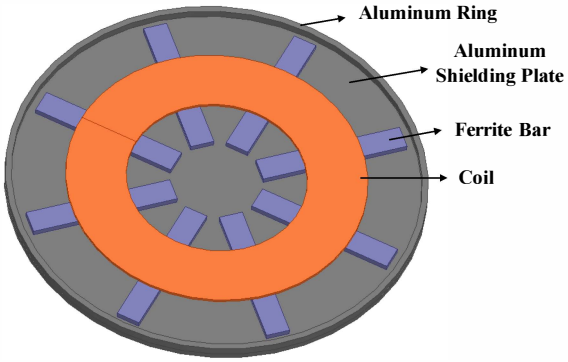


Fig. 2. Structure of a circular power pad.

The structure of a typical circular pad and its components are depicted in Fig. 2. These pads are comprised of a coil, ferrite bars and aluminum shielding plate. These types of power pads are relatively thin compared to conventional core topologies. Also, they are lighter than conventional circular pad designs that use solid ferrite discs.

## III. Finite Element Modeling of IPT Systems

The calculation of different parameters related to IPT systems is essential for design optimization purposes. Due to complexity of IPT systems, finding analytical solutions for electromagnetic field distribution may not be possible. However, different numerical analysis methods can be employed for electromagnetic field analysis. In this study finite element analysis (FEA) using ANSYS software is used for electromagnetic field analysis of any IPT system design. A 2D quasi-static electromagnetic finite element model is used for FEAs. A Dirichlet boundary condition is used at the outer boundaries of the FE models to model the space out of the drawing region as infinitely large. The coils are modeled as a stranded coil domain. Fig. 2 shows a 2D FE model of a circular power pad.

### A. 2D Quasi-Static FEA Formulation

The 2D finite element method for solving the eddy current problem uses the quasi-static magnetic vector potential PDE formulation given by:

$$\nabla \times (v\,(\nabla \times A)) = J_e - j\omega\sigma A \tag{1}$$

### B. Coil Losses

In the design optimization of circular power pads for IPT systems, accurate prediction of high-frequency coil loss is of great importance. Eddy-current winding loss increases rapidly with frequency, and can be divided into skin-effect loss and proximity-effect loss. Due to the complexity of pad geometries and interactions between conductors in windings, it is difficult to find a general analytical solution for the eddy current losses in coils. The coils are constructed using Litz wire to minimize the eddy current loss due to skin effect and proximity effect. The Litz wire consists of many thin wire strands,

individually insulated and twisted or woven together, following one of several carefully prescribed patterns, often involving several groups of twisted wires are twisted together. The losses associated with the coils can be computed as follows:

$$P_{coil} = F_r i_{rms}^2 R_{dc} \tag{2}$$

where $F_r$ is the ratio of AC resistance ($R_{ac}$) to DC resistance ($R_{dc}$), which accounts for skin and proximity coil losses, given a sinusoidal current with RMS amplitude $i_{rms}$. The loss factor $F_r$ can be approximated as follows [21]:

$$F_r = 1 + \frac{\pi^2 \omega^2 \mu_0^2 N^2 n^2 d_c^2 k}{768 \rho_c^2 g^2} \tag{3}$$

where $\omega$ is the angular frequency of a sinusoidal current, $n$ is the number of strands, $N$ is the number of turns, $d_c$ is the diameter of the copper in each strand, $\rho_c$ is the resistivity of the copper conductor, $g$ is the air gap between transmitter and receiver power pads, and $k$ is a factor accounting for field distribution in multiwinding coils, normally equal to one.

### C. Ferrite Core Losses

The ferrite cores, which are used to increase the magnetic coupling between the power pads, produce losses due to high frequency magnetic flux. Therefore, calculation of losses in ferrite cores is essential. The losses in the ferrite cores can be calculated using Steinmetz equation as follows:

$$P_{core} = k f^{\alpha} \hat{B}^{\beta} \tag{4}$$

where $P$ is the time-average core loss per unit volume, $\hat{B}$ is the peak flux density, $f$ is the frequency of sinusoidal excitation, and $k$, $\alpha$, $\beta$ are Steinmetz constants, which can be found by curve fitting. Since (4) gives the unit volume loss, by integrating this equation over the ferrites volume in any power pad structure, the total core loss can be calculated.

### D. Shielding Plate Losses

At the boundaries, where the magnetic field penetrates only a short distance into the boundary, the Impedance Boundary Condition (IBC) is used for approximating the magnetic field penetration into the boundary. IBC is a combination of Dirichlet and Neumann boundary conditions. The IBC can be used to model a bounded domain as an unbounded region and it is a valid approximation if the skin depth is small compared to the size of the conductor. The penetration depth $\delta$ is measured using the following equation:

$$\delta = \sqrt{\frac{2}{\omega \mu \sigma}} \tag{5}$$

Since in circular power pads, shielding plates are made of aluminum and the penetration depth of aluminum at high frequencies is much smaller than the dimensions of the shielding plates (for example, at 20 kHz is less than 1 mm), in 2D FEM model of the IPT system, IBC can be applied to the exterior boundaries of the shielding plates. This will further simplify the FEM model by reducing the number of required mesh elements. Also the plate losses can be calculated as follows [22]:

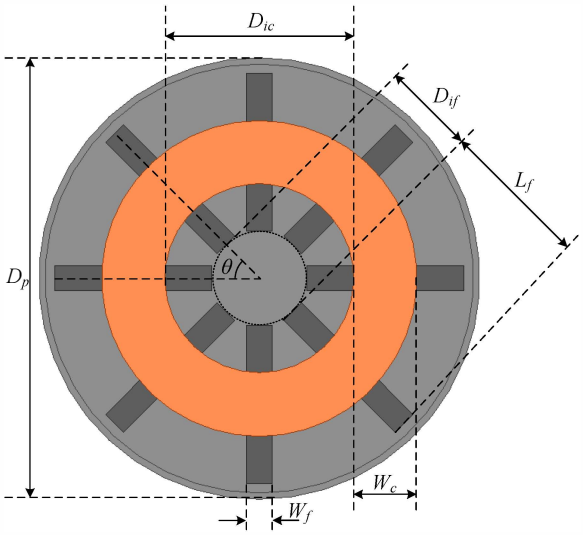


Fig. 3. Geometrical parameters of a circular power pad.

$$P_{plate} = \sqrt{\frac{\omega \mu}{2\sigma}} H_{rms}^2 \tag{6}$$

## IV. Design Optimization

The power output of an IPT system can be calculated as follows [23]:

$$P_{out} = \omega I_1^2 \frac{M^2}{L_2} Q_2 \tag{7}$$

where $\omega$ is the angular frequency of the primary pad current $I_1$, $M$ is the mutual inductance between the pads and $L_2$ is the inductance of the secondary pad with the primary pad open-circuited. Equation (7) shows that the output power can be determined based on the power supply current and frequency ($\omega I_1^2$), magnetic coupling between the pads ($M^2/L_2$) and switch-mode controller ($Q_2$). The term $\omega I_1^2 Q_2$ is limited to the operational limitations of the power electronic converters. Therefore, it is essential that the power pads have a high magnetic coupling between the pads to ensure the overall feasibility, cost effectiveness, and efficiency of the IPT system. The magnetic coupling between pads ($M^2/L_2$) is determined by the vertical and horizontal separation between the pads and the structure of the pads. The VA rating of each pad can be calculated as follows [23]:

$$S_{pad} = P_{out} \sqrt{Q^2 + 1} \tag{8}$$

Using the rated VA of each pad given by (8), the rated current can be calculated. Thereby, the magnetic structure can be analyzed using the FEA based on electrical and geometrical parameters. The objective functions and constraints of the multi-objective optimization problem are presented in the following sections.

### A. Optimization Objectives

The proposed optimization of circular pads includes the following objectives:

*1) Total Loss ($P_t$):* This objective function incorporates all the losses in the coils, ferrite cores, shielding plates and compensation capacitors both in the primary and secondary sides, which are all described in Section III. The total losses are dependent to $\bar{D}$ and $\bar{E}$ vectors and can be calculated as follows:

$$P_t(\bar{D}, \bar{E}) = P_{coil} + P_{core} + P_{plate} \tag{9}$$

where $P_{coil}, P_{core}, P_{plate}$ can be calculated using (2), (4), and (6) respectively.

*2) Total Cost ($C_t$):* The total material cost of each circular pad can be calculated by calculating the length of Litz wire, ferrite core volume, and shielding plate area as follows:

$$C_t(\bar{D}) = \pi(D_c + W_c)N_c C_c + L_f W_f H_f N_f C_f + \pi \frac{D_p^2}{4} C_p \tag{10}$$

where vector $\bar{D}$ contains the geometrical parameters of the circular power pad and vector $\bar{E}$ contains the electrical parameters of the primary converter, which both are defined in Table I, and $C_c$, $C_f$, $C_p$ are the cost coefficients of the Litz wire, ferrite core and aluminum plate respectively.

*3) Horizontal Misalignment Tolerance ($D_h$):* The horizontal misalignment tolerance for each pad structure can be evaluated using FEA. This can be carried out by calculation of the magnetic coupling between two power pads at different horizontal displacement points. The maximum feasible horizontal displacement is defined as $D_h$.

### B. Optimization Constraints

There are different types of constraints, which limit the search space of the optimization problem. These constraints include geometric constraints, EMF exposure limitations, as well as converter limitations.

*1) Geometric Constraints:* The geometric constraints are determined based on the space limitations for the transmitter and receiver pads under the electric vehicle. Therefore, the outer diameter of the pads should be less than a maximum allowable value:

$$D_p \leq D_{max} \tag{11}$$

*2) EMF Exposure Limitations:* The EMF emission of the IPT system should be in compliance with standards such as those defined by International Commission on Non-Ionizing Radiation Protection (ICNIRP).

$$EMF(\bar{D}, \bar{E}) \leq EMF_{max}(f) \tag{12}$$

where $EMF_{max}(f)$ is the maximum $EMF$ allowed at frequency $f$.

TABLE I
THE COMPONENTS OF DIMENSIONS VECTOR $\bar{D}$ AND ELECTRICAL PARAMETERS VECTOR $\bar{E}$.

| Parameter | Description |
|---|---|
| $D_p$ | shielding plate diameter |
| $D_{ic}$ | internal diameter of the coil |
| $W_c$ | width of the coil |
| $d_c$ | diameter of the Litz wire |
| $N_c$ | number of turns |
| $D_{if}$ | internal diameter of the ferrite ends |
| $L_f$ | ferrite bar length |
| $W_f$ | ferrite bar width |
| $H_f$ | ferrite bar thickness |
| $N_f$ | no. of ferrite bars |
| $f$ | operating frequency |
| $I_1$ | primary RMS current |

*3) Converter Limitations:* The VA rating of the power converters as well as operating frequency are limited by those power electronic switches presently available. In practical applications, the operating quality factors $Q$, is constrained to 4-10:

$$4 \leq Q_1, Q_2 \leq 10 \tag{13}$$

This limitations are due to component VA ratings and tolerances of the power converter.

### C. Multi-Objective Optimization Formulation

The multi-objective optimization problem (MOP) can be formulated as follows:

$$\min \bar{F}(\bar{D}, \bar{E}) = (P_t, C_t, D_h) \tag{14}$$

subject to constraints which are defined in IV.B. Different methods can be used to solve the MOP, such as genetic algorithms (GA), differential evolution (DE), particle swarm optimization (PSO) [24]. In this study, a elitist non-dominated sorting genetic algorithm (NSGA-II) is used to find the pareto optimal solutions for the MOP. An elitist GA always favors individuals with better fitness rank and as a result, it converges relatively fast [25].

## V. CASE STUDY ANALYSIS

A 10 kW electric vehicle battery charger IPT system with 200 mm air gap is investigated as the case study. The power pads are assumed to have a diameter no more than 750 mm. The primary converter can provide 64 A within the frequency range of 10-85 kHz with operating quality factors of 4-10. Also, the EMF emissions of the IPT system is limited to 5 mG to meet human exposure regulations in compliance with standards, as defined by International Commission on Non-Ionizing Radiation Protection (ICNIRP) [26]. Also, the ferrite bars are selected as MnZn N87 material. The specifications and constraints of the case study IPT system is presented in Table II. The cost coefficients which are used to evaluate the cost of the power pads are presented in Table III.

MATLAB software is used to carry out the NSGA-II optimization coupled with 2D FEA using ANSYS software. Each FEA model is set to have at least 150 k elements to ensure the desired accuracy in electromagnetic field computations. A

TABLE II
DESIGN SPECIFICATIONS AND CONSTRAINTS THE IPT SYSTEM WITH CIRCULAR POWER PADS.

| Description | Value |
|---|---|
| Air gap ($g$) | 200 mm |
| Output power ($P_2$) | 10 kW |
| Frequency range ($f_{min} - f_{max}$) | 10 kHz-85 kHz |
| Max. primary current ($I_1$) | 64 A |
| Max. pad diameter ($D_p$) | 750 mm |
| Max. EMF ($EMF_m$) | 5 mG |
| Operating quality factor range | 4 - 10 |

TABLE III
THE COEFFICIENTS USED FOR COST CALCULATION.

| Coefficient | Description | Value |
|---|---|---|
| $C_c$ | Litz wire cost in unit length ($/m) | 2.04 |
| $C_f$ | Ferrite cost in unit volume ($/cm$^3$) | 0.18 |
| $C_p$ | Aluminum plate cost in unit area ($/m$^2$) | 333.68 |

TABLE IV
MULTI-OBJECTIVE OPTIMIZATION PARAMETERS.

| Description | Value |
|---|---|
| Population size | 60 |
| Cross-over probability | 0.8 |
| Mutation probability | 0.8 |
| Number of generations | 104 |
| Number Pareto-optimal points | 21 |
| Total optimization time | 308 min. |

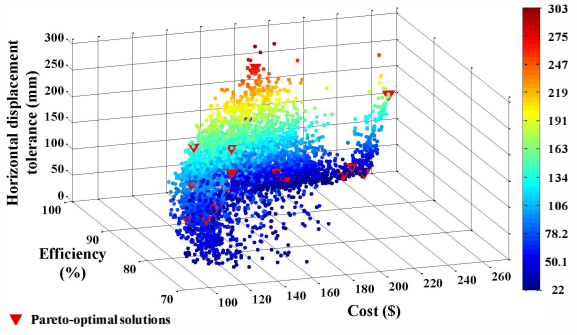


Fig. 4. The plot of horizontal displacement vs. efficiency and cost within the search space of the multi-objective optimization.

computer with Intel Core i7-4770 3.4 GHz CPU and 4 GB of RAM is employed for computations. The parameters of the optimization are presented in Table IV. The optimization is completed in 308 minutes with 104 generation. The Pareto-optimal solutions are presented in Table V. This table presents 21 Pareto-optimal solutions with corresponding design parameters and the values of the objective functions. Any of these Pareto-optimal solutions can be selected based on the IPT system design priorities. For example, when the cost of the IPT system is not of interest, solution no. 17 in Table V can be considered as a highly efficient (96.6%) design, which has a high tolerance to horizontal displacement (219.9 mm). In the case where horizontal displacement tolerance is of higher priority, solution no. 18 would be an optimal design with 350.7 mm horizontal displacement tolerance, efficiency of 92.5% and $175.5 cost.

TABLE V
PARETO-OPTIMAL SOLUTIONS FOR A 10KW ELECTRIC VEHICLE BATTERY CHARGER IPT SYSTEM.

| | Design parameters | | | | | Objective functions | | |
|---|---|---|---|---|---|---|---|---|
| No. | $L_f$ | $D_{if}$ | $W_c$ | $D_{ic}$ | $f$(kHz) | $\eta$(%) | Cost($) | $D_h$ |
| 1 | 117.4 | 78.6 | 71.6 | 104.7 | 62.7 | 80.3 | 109.2 | 89.2 |
| 2 | 136.4 | 20.0 | 67.1 | 110.5 | 63.8 | 79.6 | 118.9 | 90.5 |
| 3 | 222.1 | 70.1 | 122.3 | 187.4 | 24.0 | 96.4 | 240.6 | 49.1 |
| 4 | 158.4 | 67.1 | 96.8 | 139.1 | 23.1 | 92.9 | 159.9 | 54.5 |
| 5 | 200.0 | 55.7 | 100.9 | 150.8 | 22.8 | 95.1 | 199.0 | 40.7 |
| 6 | 215.5 | 97.7 | 123.7 | 169.1 | 28.7 | 96.2 | 235.0 | 31.7 |
| 7 | 174.2 | 64.0 | 110.6 | 109.3 | 50.9 | 94.4 | 175.0 | 205.3 |
| 8 | 133.2 | 79.1 | 77.9 | 115.2 | 56.2 | 87.1 | 126.7 | 120.2 |
| 9 | 188.6 | 58.7 | 109.2 | 148.4 | 43.3 | 94.9 | 193.6 | 64.9 |
| 10 | 192.0 | 81.9 | 107.5 | 117.6 | 37.0 | 94.8 | 192.2 | 107.5 |
| 11 | 142.1 | 73.1 | 62.7 | 104.3 | 76.4 | 80.1 | 125.9 | 115.0 |
| 12 | 173.6 | 35.4 | 78.1 | 123.0 | 53.7 | 90.5 | 157.6 | 171.7 |
| 13 | 165.7 | 72.8 | 89.9 | 139.4 | 32.7 | 92.6 | 162.6 | 79.3 |
| 14 | 149.3 | 61.2 | 127.5 | 115.6 | 31.3 | 93.8 | 165.0 | 83.8 |
| 15 | 231.5 | 94.5 | 120.5 | 167.2 | 21.7 | 96.6 | 248.5 | 28.4 |
| 16 | 140.8 | 57.9 | 78.6 | 107.8 | 83.2 | 88.1 | 130.2 | 203.8 |
| 17 | 240.6 | 62.3 | 124.5 | 207.2 | 25.0 | 96.6 | 263.2 | 219.9 |
| 18 | 190.3 | 47.2 | 84.5 | 113.8 | 85.0 | 92.5 | 175.5 | 350.7 |
| 19 | 222.1 | 70.1 | 122.3 | 187.4 | 24.0 | 96.4 | 240.7 | 49.7 |
| 20 | 136.4 | 20.0 | 67.2 | 110.6 | 63.8 | 79.6 | 119.0 | 90.7 |
| 21 | 239.8 | 62.0 | 124.1 | 207.7 | 25.4 | 96.5 | 262.5 | 218.3 |

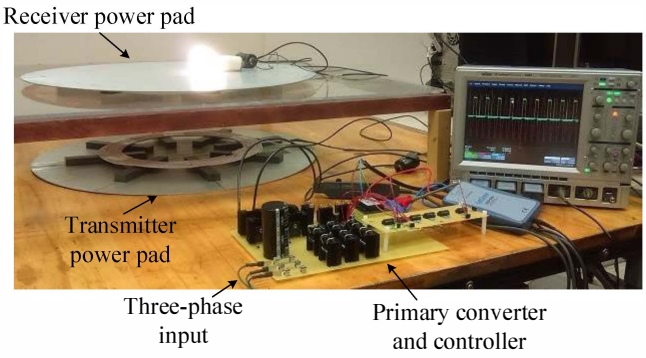


Fig. 5. The IPT test-bed consisting of two circular power pads.

TABLE VI
EXPERIMENTAL SPECIFICATIONS AND TEST RESULTS ON THE SAMPLE CIRCULAR POWER PADS.

| Description | Value |
|---|---|
| Output power | 1 kW |
| Frequency | 35 kHz |
| Compensation capacitors | $0.12\mu F$ |
| Self-inductance of the pads | $172\mu H$ |
| Efficiency of the pads | 89% |
| Horizontal misalignment tolerance | 115 mm |

In order to validate the theoretical computations, two identical circular power pads based on the case no. 10 of Table V are built and tested experimentally. The experimental setup is shown in Fig. 5. The setup consists of the two circular power pads which form the transmitter and receiver structures, a three-phase AC/DC/AC primary converter which is connected to a three-phase source. Although the power pads are designed for 10 kW output power, due to practical limitations the tests are carried out at 1 kW output power. The specifications of the setup and the test results are presented in Table VI. By comparing Table V and VI, it can be seen the difference between theoretical and measurements are less than 7%.

## VI. Conclusion

The proposed multi-objective optimization method based on FEA provides an effective tool for the optimal design of highly-efficient and cost-effective circular power pads with high flexibility to misalignments in contactless electric vehicle battery charging systems. The efficiency, cost and horizontal misalignment capability, which are all of a great importance in IPT systems, are considered as the objective functions. Also, practical limitations associated with power electronic converters are defined as constraints. The optimal design of the pads can be selected between Pareto-optimal solutions based on the prioritization of the objectives. The Pareto-optimal solutions comply with ICNIRP standard and are compatible with power converters to work in operational limits. Experimental test results on sample power pads have validated the theoretical computations with maximum 7% difference.

## References


[1] J. de Boeij, E. A. Lomonova, and A. J. A. Vandenput, "Optimization of contactless planar actuator with manipulator," *IEEE Transactions on Magnetics*, vol. 44, no. 6, pp. 1118–1121, June 2008.

[2] P. Sergeant and A. V. D. Bossche, "Inductive coupler for contactless power transmission," *IET Electric Power Applications*, vol. 2, no. 1, pp. 1–7, Jan 2008.

[3] F. Sato, T. Nomoto, G. Kano, H. Matsuki, and T. Sato, "A new contactless power-signal transmission device for implanted functional electrical stimulation (fes)," *IEEE Transactions on Magnetics*, vol. 40, no. 4, pp. 2964–2966, July 2004.

[4] Q. Chen, S. C. Wong, C. K. Tse, and X. Ruan, "Analysis, design, and control of a transcutaneous power regulator for artificial hearts," *IEEE Transactions on Biomedical Circuits and Systems*, vol. 3, no. 1, pp. 23–31, Feb 2009.

[5] G. A. Covic and J. T. Boys, "Modern trends in inductive power transfer for transportation applications," *IEEE Journal of Emerging and Selected Topics in Power Electronics*, vol. 1, no. 1, pp. 28–41, March 2013.

[6] C.-S. Wang, O. H. Stielau, and G. A. Covic, "Design considerations for a contactless electric vehicle battery charger," *IEEE Transactions on Industrial Electronics*, vol. 52, no. 5, pp. 1308–1314, Oct 2005.

[7] J. Sallan, J. L. Villa, A. Llombart, and J. F. Sanz, "Optimal design of icpt systems applied to electric vehicle battery charge," *IEEE Transactions on Industrial Electronics*, vol. 56, no. 6, pp. 2140–2149, June 2009.

[8] R. Bosshard, J. Kolar, J. Muhlethaler, I. Stevanovic, B. Wunsch, and F. Canales, "Modeling and $\eta$ - $\alpha$ -pareto optimization of inductive power transfer coils for electric vehicles," *Emerging and Selected Topics in Power Electronics, IEEE Journal of*, vol. 3, no. 1, pp. 50–64, March 2015.

[9] M. Budhia, G. Covic, and J. Boys, "Design and optimization of circular magnetic structures for lumped inductive power transfer systems," *Power Electronics, IEEE Transactions on*, vol. 26, no. 11, pp. 3096–3108, Nov 2011.

[10] P. Raval, D. Kacprzak, and A. P. Hu, "Analysis of flux leakage of a 3-d inductive power transfer system," *IEEE Journal of Emerging and Selected Topics in Power Electronics*, vol. 3, no. 1, pp. 205–214, March 2015.

[11] S. Wang and D. G. Dorrell, "Copper loss analysis of ev charging coupler," *IEEE Transactions on Magnetics*, vol. 51, no. 11, pp. 1–4, Nov 2015.

[12] J. Acero, C. Carretero, I. Lope, R. Alonso, . Lucia, and J. M. Burdio, "Analysis of the mutual inductance of planar-lumped inductive power transfer systems," *IEEE Transactions on Industrial Electronics*, vol. 60, no. 1, pp. 410–420, Jan 2013.

[13] S. Wang and D. G. Dorrell, "Loss analysis of circular wireless ev charging coupler," *IEEE Transactions on Magnetics*, vol. 50, no. 11, pp. 1–4, Nov 2014.

[14] S. Y. Choi, J. Huh, W. Y. Lee, and C. T. Rim, "Asymmetric coil sets for wireless stationary ev chargers with large lateral tolerance by dominant field analysis," *IEEE Transactions on Power Electronics*, vol. 29, no. 12, pp. 6406–6420, Dec 2014.

[15] D. A. G. Pedder, A. D. Brown, and J. A. Skinner, "A contactless electrical energy transmission system," *IEEE Transactions on Industrial Electronics*, vol. 46, no. 1, pp. 23–30, Feb 1999.

[16] C.-G. Kim, D.-H. Seo, J.-S. You, J.-H. Park, and B. H. Cho, "Design of a contactless battery charger for cellular phone," *IEEE Transactions on Industrial Electronics*, vol. 48, no. 6, pp. 1238–1247, Dec 2001.

[17] G. A. J. Elliott, G. A. Covic, D. Kacprzak, and J. T. Boys, "A new concept: Asymmetrical pick-ups for inductively coupled power transfer monorail systems," *IEEE Transactions on Magnetics*, vol. 42, no. 10, pp. 3389–3391, Oct 2006.

[18] H. Sakamoto, K. Harada, S. Washimiya, K. Takehara, Y. Matsuo, and F. Nakao, "Large air-gap coupler for inductive charger [for electric vehicles]," *IEEE Transactions on Magnetics*, vol. 35, no. 5, pp. 3526–3528, Sep 1999.

[19] S. Valtchev, B. Borges, K. Brandisky, and J. B. Klaassens, "Resonant contactless energy transfer with improved efficiency," *IEEE Transactions on Power Electronics*, vol. 24, no. 3, pp. 685–699, March 2009.

[20] X. Liu and S. Y. Hui, "Optimal design of a hybrid winding structure for planar contactless battery charging platform," *IEEE Transactions on Power Electronics*, vol. 23, no. 1, pp. 455–463, Jan 2008.

[21] C. R. Sullivan, "Optimal choice for number of strands in a litz-wire transformer winding," *IEEE Transactions on Power Electronics*, vol. 14, no. 2, pp. 283–291, Mar 1999.

[22] K. Ishibashi, "Eddy current analysis by boundary element method utilizing impedance boundary condition," *IEEE Transactions on Magnetics*, vol. 31, no. 3, pp. 1500–1503, May 1995.

[23] J. T. Boys, G. A. Covic, and A. W. Green, "Stability and control of inductively coupled power transfer systems," *IEE Proceedings - Electric Power Applications*, vol. 147, no. 1, pp. 37–43, Jan 2000.

[24] I. Giagkiozis and P. Fleming, "Methods for multi-objective optimization: An analysis," *Information Sciences*, vol. 293, pp. 338 – 350, 2015. [Online]. Available: http://www.sciencedirect.com/science/article/pii/S0020025514009074

[25] K. Deb, *Multi-objective optimization using evolutionary algorithms*. John Wiley & Sons, 2001, vol. 16.

[26] J. Lin, R. Saunders, K. Schulmeister, P. Söderberg, A. Swerdlow, M. Taki, B. Veyret, G. Ziegelberger, M. H. Repacholi, R. Matthes *et al.*, "Icnirp guidelines for limiting exposure to time-varying electric and magnetic fields (1 hz to 100 khz)." *Health Physics*, vol. 99, pp. 818–836, 2010.


978-1-4799-8397-1/16/$31.00 © 2016 IEEE